

Offboard Occupancy Refinement with Hybrid Propagation for Autonomous Driving

Hao Shi^{1,*}, Song Wang^{3,*}, Jiaming Zhang⁴, Xiaoting Yin¹, Zhongdao Wang⁵, Guangming Wang⁶, Jianke Zhu³, Kailun Yang², and Kaiwei Wang¹

Abstract—Vision-based occupancy prediction, also known as 3D Semantic Scene Completion (SSC), presents a significant challenge in computer vision. Previous methods, confined to onboard processing, struggle with simultaneous geometric and semantic estimation, continuity across varying viewpoints, and single-view occlusion. Our paper introduces OccFiner, a novel *offboard* framework designed to enhance the accuracy of vision-based occupancy predictions. OccFiner operates in two hybrid phases: 1) a *multi-to-multi local propagation network* that implicitly aligns and processes multiple local frames for correcting onboard model errors and consistently enhancing occupancy accuracy across all distances. 2) the *region-centric global propagation*, focuses on refining labels using explicit multi-view geometry and integrating sensor bias, especially to increase the accuracy of distant occupied voxels. Extensive experiments demonstrate that OccFiner improves both geometric and semantic accuracy across various types of coarse occupancy, setting a new state-of-the-art performance on the SemanticKITTI dataset. Notably, OccFiner elevates vision-based SSC models to a level even surpassing that of LiDAR-based onboard SSC models. Furthermore, OccFiner is the first to achieve automatic annotation of SSC in a purely vision-based approach. Quantitative experiments prove that OccFiner successfully facilitates occupancy data loop-closure in autonomous driving. Additionally, we quantitatively and qualitatively validate the superiority of the offboard approach on city-level SSC static maps. The source code will be made publicly available at <https://github.com/MasterHow/OccFiner>.

Index Terms—Semantic Scene Completion, 3D Occupancy Prediction, Offboard Perception, Data Loop-Closure.

I. INTRODUCTION

Vision-based Occupancy Prediction, often referred to as Semantic Scene Completion (SSC), aims to accurately reconstruct the geometry and semantics of a 3D scene from image captures [1], providing critical location and semantic information for safe navigation in autonomous driving. Compared

to LiDAR solutions, camera-based systems offer the benefits of being lightweight, cost-effective, and easy to deploy and maintain.

However, vision-based SSC has historically lagged in accuracy compared to LiDAR due to two main limitations: 1) The depth measurement of monocular cameras lacks the precision of LiDAR systems, requiring onboard vision-based SSC methods to struggle with both geometry and semantics. 2) Onboard models are limited to processing a restricted number of local frames, impacting accuracy and multi-view continuity. This issue manifests as unreliable estimations and discontinuities across viewpoints in geometry and semantics. As illustrated in Fig. 1, most SSC efforts are focused on *onboard* settings [1]–[8], *i.e.*, data calculation and feedback occur on the vehicle itself. However, integrating data into *offboard* systems is critical for identifying and rectifying potential model deficiencies, achieving data loop-closure, and enabling system self-evolution, which are essential for a wide range of intelligent transportation applications [9]. This approach solves the distribution shift between training and deployment and allows training to be scaled both safely and cost-effectively [10]. While offboard systems offer refined evaluation of onboard model performance, essential for the data loop-closure in autonomous driving [9]–[11], and well-studied in 3D detections [12]–[15], their potential in SSC remains under-explored.

Given such limitations of inferior performance and onboard SSC settings, we propose the first *offboard* SSC framework, **OccFiner**, a novel approach that involves additional computation and refinement of on-vehicle predictions at a data center but greatly boosts the prediction reliability. The objective is to significantly enhance the reliability of vision-based SSC. By doing so, the constructed 3D SSC map can be reliably used repeatedly after a one-time low-cost acquisition with only cameras. This approach enhances auto-labeling by leveraging aggregated and diverse data from multiple sources, significantly reducing manual annotation efforts and improving labeling accuracy for large-scale 3D scene understanding [9]–[11] in autonomous driving.

Specifically, we consider two primary error sources in addressing the inaccuracies of vision-based SSC: the prediction bias error introduced by the onboard model, and the measurement bias from the camera capture process. OccFiner decouples these two heterogeneous error sources and uses a two-stage hybrid process to process them separately: 1) *Multi-to-Multi Local Propagation*. In the initial stage, OccFiner addresses prediction bias errors from the onboard model.

This work was supported in part by the National Natural Science Foundation of China (NSFC) under Grant No. 12174341, and in part by Shanghai SUPREMIN Technology Company Ltd. (*Corresponding authors: Kaiwei Wang; Kailun Yang.*)

¹H. Shi, X. Yin, and K. Wang are with the State Key Laboratory of Extreme Photonics and Instrumentation and the National Engineering Research Center of Optical Instrumentation, Zhejiang University, Hangzhou 310027, China.

²K. Yang is with the School of Robotics and the National Engineering Research Center of Robot Visual Perception and Control Technology, Hunan University, Changsha 410082, China.

³S. Wang and J. Zhu are with the College of Computer Science and Technology, Zhejiang University, Hangzhou 310027, China.

⁴J. Zhang is with the Institute for Anthropomatics and Robotics, Karlsruhe Institute of Technology, 76131 Karlsruhe, Germany.

⁵Z. Wang is with Huawei Noah's Ark Lab.

⁶G. Wang is with the Department of Engineering, University of Cambridge, Cambridge CB2 1PZ, U.K.

*These authors contributed equally.

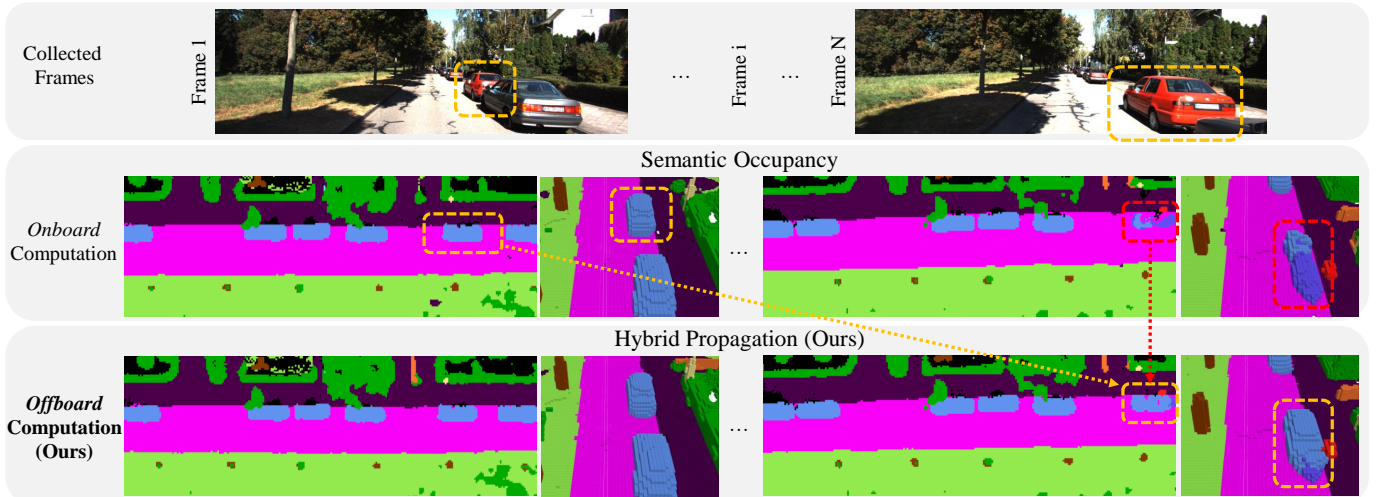


Fig. 1. Current *onboard* methods generate unreliable occupancy predictions that are inconsistent across different viewpoints. In contrast, our *offboard* framework constructs a unified and multi-view consistent occupancy map with higher accuracy.

We implement an error compensation model that processes inputs from off-the-shelf SSC models [1], [2], [4]. This model uniquely encodes relative spatial coordinates within a local window, facilitating the propagation of geometric and semantic cues by a newly proposed DualFlow4D transformer. This approach effectively enhances the accuracy of occupancy predictions at varying distances. 2) *Region-centric Global Propagation*. The second stage focuses on measurement errors from camera captures. Here, OccFiner employs explicit multi-view geometry to register and aggregate data across the entire scene, incorporating sensor bias weighting in the process. Compared with the simple accumulation of multi-frame averages, our region-centric voting strategy yields a more accurate SSC map. By integrating local implicit error compensation and non-local explicit information propagation from various viewpoints, OccFiner effectively addresses onboard bias, multi-view consistency, and single-view occlusions, thereby naturally enhancing the reliability and robustness of scene understanding.

To the best of our knowledge, we are the first to introduce offboard refinement for SSC. Our method, termed OccFiner, enables seamless integration across various SSC models and datasets as a plug-and-play solution. For 3D semantic scene completion on the SemanticKITTI dataset [16], OccFiner has demonstrated remarkable performance, surpassing VoxFormer by 3.67% in mIoU, which makes a 26.99% relative improvement and ranks first on the test leaderboard among all vision-based methods. Surprisingly, OccFiner also works well for LiDAR-based SSC [17] with minor changes, leading to a new state-of-the-art of 37.82% in mIoU, achieving a 9.5% improvement compared with the best benchmark result.

To summarize, we deliver the following contributions:

- We are the first to explore the problem of learning to generate high-quality vision-oriented SSC maps offboard.
- We propose OccFiner, an effective offboard occupancy refinement framework with hybrid propagation to build multi-view consistent SSC maps.
- OccFiner sets new state-of-the-art performances in both camera-based and LiDAR-based SSC. For the first time, the accuracy of the camera-based SSC method surpasses that of the classical onboard LiDAR-based method [18].
- We demonstrate that offboard occupancy can successfully facilitate pure vision-based automatic annotation and help achieve a closed data loop for autonomous driving.
- We construct city-level occupancy maps and prove that the offboard approach is also beneficial for large-scale global SSC mapping.

II. RELATED WORK

A. 3D Semantic Scene Completion

Semantic Scene Completion (SSC), also known as Semantic Occupancy Prediction, aims at concurrently estimating the geometry and semantics of a surrounding scene. The first effort SSCNet [18] lays the foundation for this field by defining the SSC task and introducing a method for estimating the structure and semantics of indoor scenes from a singular depth image input. Recognizing the critical role of SSC-based perception in the realm of autonomous driving, researchers have increasingly turned their attention to its applications in outdoor scenes after the release of the large-scale outdoor benchmark SemanticKITTI [16]. The predominant works in this area can be broadly categorized based on the input modality: LiDAR-based SSC [2], [17], [19]–[24] and vision-based SSC [1], [3], [25]–[36]. Additionally, recent research expands into several novel areas within SSC including the world model [37], 3D object detection [38]–[44], multimodal parsing [5], [45]–[52], self-supervised prediction [53]–[57], open-vocabulary recognition [58], [59], dense top-view understanding [60]–[62], V2X collaboration [63]–[65], as well as various benchmarks [66]–[68]. However, the majority of previous studies have concentrated on methodological design within onboard settings, where observations across different viewpoints often exhibit notable discontinuities. In contrast, OccFiner shifts focus to the offboard setting, aiming to rectify errors inherent in onboard models and to aggregate long-term geometric and semantic cues. Our approach contributes to data closure in autonomous driving, addressing a crucial aspect that has been largely overlooked in previous SSC research.

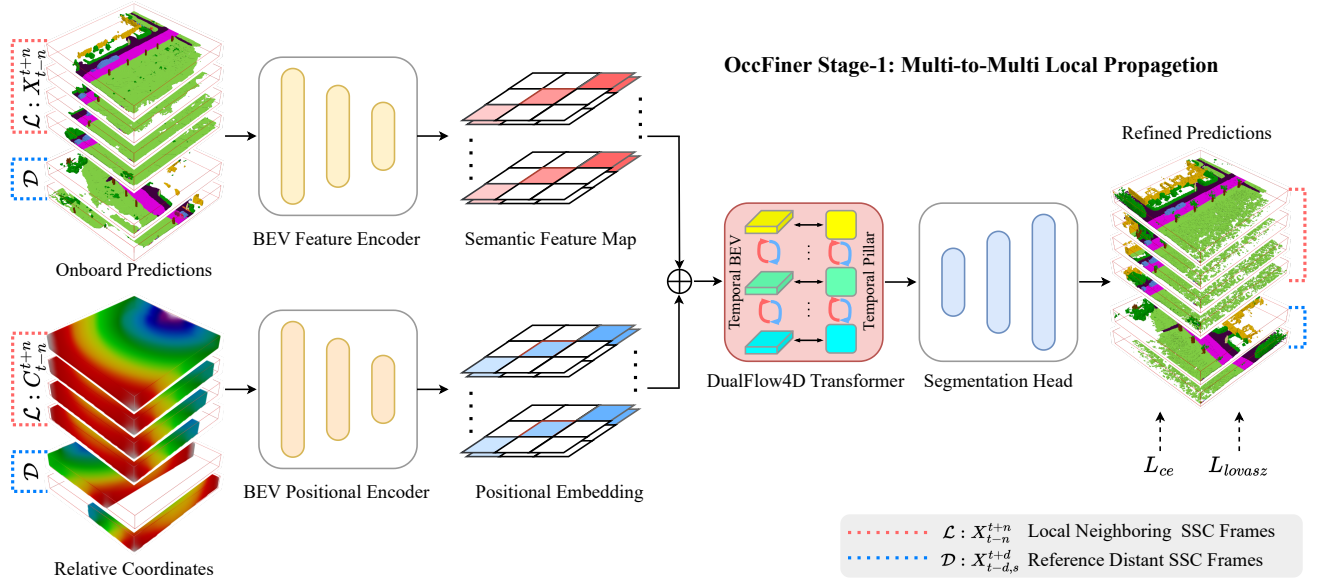


Fig. 2. **Overview of the proposed multi-to-multi local propagation network.** It accepts multiple onboard predictions and relative coordinates as input. This network adeptly executes error compensation and facilitates the implicit local propagation, improving SSC quality across various distances.

B. Offboard 3D Perception

Perception in autonomous driving scenarios necessitates extensive data annotation and training [69]–[71]. Since LiDAR can provide accurate range information in 3D space, researchers explore its sequence learning in semantic segmentation [72], [73], object detection [74], [75] and tracking [76] to obtain better performance. The sequential characteristics of LiDAR scans are further studied in offboard 3D object detection [12]–[15] to reduce annotation costs. 3DAL [12] formulates the problem of offboard 3D object detection and proposes an *object-centric* auto-labeling detector. CTRL [14] adheres to the principle of *track-centric* and elevates the accuracy of auto-labeling, surpassing manual annotation in some scenarios. The aforementioned methods are all designed for LiDAR point cloud, attributed to the ease of accumulating 3D spatial information compared to images. MV-Map [77] provides a *region-centric* fusion solution for high-definition maps with camera data as inputs while it only processes limited traffic elements on the bird’s eye view plane. To address the above challenges, We design the first hybrid propagation pipeline (OccFiner) for offboard semantic scene completion (SSC). OccFiner can process the SSC predictions from either cameras or LiDAR and provide high-quality occupancy information for autonomous vehicles, which holds significant importance in auto-labeling and data closure in pure visual perception.

III. APPROACH

A. Overview

The OccFiner framework, designed for offboard Semantic Scene Completion (SSC), operates in two distinct stages. The first stage focuses on compensating for errors in onboard model predictions, employing a multi-to-multi local propagation network to process SSC model outputs across a series of frames, utilizing both close-range and distant frames

as references. This stage effectively merges relative spatial coordinates with semantic features, employing transformer-based methods for spatio-temporal integration. The second stage of OccFiner emphasizes global semantic and geometric aggregation. It transforms refined voxel labels into semantic point clouds and applies relative poses over extended periods for precise coordinate adjustments, incorporating sensor measurement characteristics for voxel voting. This dual-stage strategy effectively combines local implicit feature propagation with global explicit semantic aggregation, forming a robust hybrid system for offboard SSC refinement.

B. Multi-to-Multi Local Propagation Network

Problem formulation: Let $X_1^T := \{X_1, X_2, \dots, X_T\}$ be an onboard SSC inference sequence of height H , width W , depth Z , and frames length T . $C_1^T := \{C_1, C_2, \dots, C_T\}$ denotes the corresponding frame-wise relative coordinates, which can be calculated by:

$$\mathbf{c}_i = (T_{li}^{cam})^{-1} (T_{cam_t}^{world})^{-1} T_{cam_t}^{world} T_{li}^{cam} \mathbf{x}_i, \quad (1)$$

where each vertex $\mathbf{x}_i \in X_i$ is projectively associated to a relative vertex $\mathbf{c}_i \in C_i$. For each relative coordinate C_i , it represents the mapping relationship between the three-dimensional coordinates of the current frame X_i and the coordinates of the pivot frame X_t . We formulate the occupancy refinement as a task that takes the onboard (X_1^T, C_1^T) pairs as input and reconstruct the SSC labels $Y_1^T = \{Y_1, Y_2, \dots, Y_T\}$. Specifically, we propose to learn a mapping function from onboard inferences X_1^T to the output $\hat{Y}_1^T := \{\hat{Y}_1, \hat{Y}_2, \dots, \hat{Y}_T\}$, such that the conditional distribution of the real data $p(Y_1^T | X_1^T)$ can be approximated by the one of generated data $p(\hat{Y}_1^T | X_1^T)$.

We conceptualize the task as a “multi-to-multi” prediction problem, focusing on the simultaneous refinement of all input SSC frames in a single feed-forward process. The intuition is that regions obscured in the current viewpoint are likely to

become visible in frames captured from a distance, particularly in scenarios involving large occlusions or when the vehicle is moving at a slower pace. In the context of multi-frame offboard SSC, it is more effective to address gaps in a target frame by leveraging content from the entire scene sequence, incorporating information from both neighboring and distant frames as conditional inputs. This approach relies on the Markov assumption [78] for simplification, which allows us to express the refinement process as:

$$p(\hat{Y}_1^T | X_1^T) = \prod_{t=1}^T p(\hat{Y}_{t-n}^{t+n} | X_{t-n}^{t+n}, X_{t-d,s}^{t+d}), \quad (2)$$

where X_{t-n}^{t+n} represents a short SSC clip of neighboring frames centered around time t with a temporal radius n . $X_{t-d,s}^{t+d}$ denotes distant frames that are randomly sampled from a distant scene range d at a rate of s . This selection of distant frames typically encompasses most of the key moments in possible viewpoints, effectively conveying long-term geometric and semantic cues of the scene.

Within this framework, offboard SSC models are tasked with not only maintaining temporal consistency in neighboring frames but also ensuring that the refined frames are coherent with the broader narrative of the scene sequence. This approach aims to enhance scene understanding by integrating both local and global temporal perspectives in the refinement process.

Network design: The overview of the proposed multi-to-multi local propagation network is shown in Fig. 2. As indicated in Eq. 2, OccFiner takes both neighboring local SSC frames X_{t-n}^{t+n} , distant reference SSC frames $X_{t-d,s}^{t+d}$, and relative coordinate $\{C_{t-n}^{t+n}, C_{t-d,s}^{t+d}\}$ as conditions, to propagate across all input frames simultaneously. Specifically, OccFiner is comprised of four integral components, including a frame-level BEV feature encoder, a parallel BEV positional encoder, a series of spatial-temporal transformers, and a frame-level segmentation head. The frame-level BEV feature encoder is architecturally configured with multiple 2D convolutions along the horizontal and vertical dimensions (X, Y), thus converting the height dimension (Z) into a feature dimension. Mirroring this, the frame-level BEV positional encoder shares the same architectural blueprint with the feature encoder, such a design choice aids in better aligning the positional and feature information, as both are processed through a similar computational pathway. At the heart of OccFiner lie the DualFlow4D transformers, tasked with learning and applying joint spatial-temporal transformations. These transformers are specifically tailored to address uncertainties and occlusions within the deep encoding space.

DualFlow4D transformer: To propagate high-fidelity features in each SSC frame, multi-layer DualFlow4D transformers are designed to search coherent contents from all the encoded features. Specifically, we propose to first search by a multi-head soft-patch-based focal attention module along BEV and temporal dimensions. We use $f_1^T = \{f_1, f_2, \dots, f_T\}$, where $f_i \in \mathbb{R}^{h \times w \times c}$ to denote the features encoded from the frame-level BEV encoder. Concurrently, $p_l \in \mathbb{R}^{T_l \times h \times w \times c}$ and $p_r \in \mathbb{R}^{T_r \times h \times w \times c}$ encapsulate the corresponding encoded local and

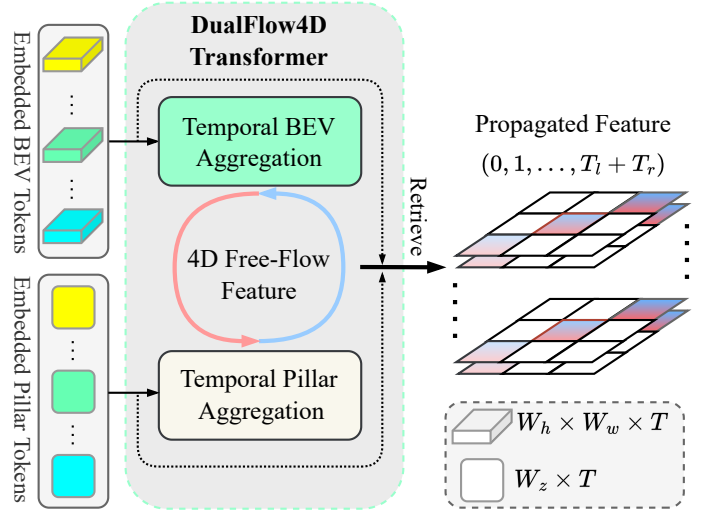


Fig. 3. **Our proposed DualFlow4D transformer block.** It engages spatiotemporal propagation within BEV space and vanilla attention to pillar tokens. This dual approach enables effective matching and flow of semantic and geometric cues for comprehensive scene understanding.

reference relative coordinates. We first use soft split to embed them into overlapped patches $P \in \mathbb{R}^{(T_l+T_r) \times W_h \times W_w \times c_e}$:

$$P = \text{SS}((f_l \oplus f_r) + (p_l \oplus p_r)), \quad (3)$$

where $\text{SS}(\cdot)$ denotes the soft split operation, which softly splits each BEV feature into overlapped patches of size $W_h \times W_w \times T$ with stride k , and flattened to a one-dimensional token, which is similar to the image splitting strategy in T2T-ViT [79]. T_l and T_r are the time dimension of local frames and reference frames, and W_h and W_w are the spatial dimension of embedded tokens. \oplus denotes the feature concatenation. The overlapped position aggregates a piece of information from different tokens, contributing to smoother semantic patch boundaries and enlarging its receptive field by fusing cues from neighboring patches.

Instead of the vanilla vision transformer [80], we use focal transformer [81] to search from both local and non-local neighbors to propagate high-fidelity BEV features. Concretely, P is linearly projected to queries Q , keys K , and values V for computing the 3D focal attention:

$$\begin{aligned} Q, K, V &= \mathcal{P}_{qkv}(\text{LN}(P)), \\ Z_{bev} &= \text{MHFA}(Q, K, V) + P, \end{aligned} \quad (4)$$

where LN and MHFA denote the layer normalization and multi-head focal attention, respectively, \mathcal{P}_{qkv} is the linear projection layer. We omit the time dimension for simplicity. The previous propagation is limited to the temporal BEV space. To ensure effective propagation in the height direction, we have additionally introduced attention along the z-axis, specifically focusing on the ‘pillar’, which refers to a voxel grid oriented along the height:

$$Z_z := \text{Attn}(Q_z, K_z, V_z) = \text{Softmax}\left(\frac{Q_z K_z^\top V_z}{\sqrt{d}}\right), \quad (5)$$

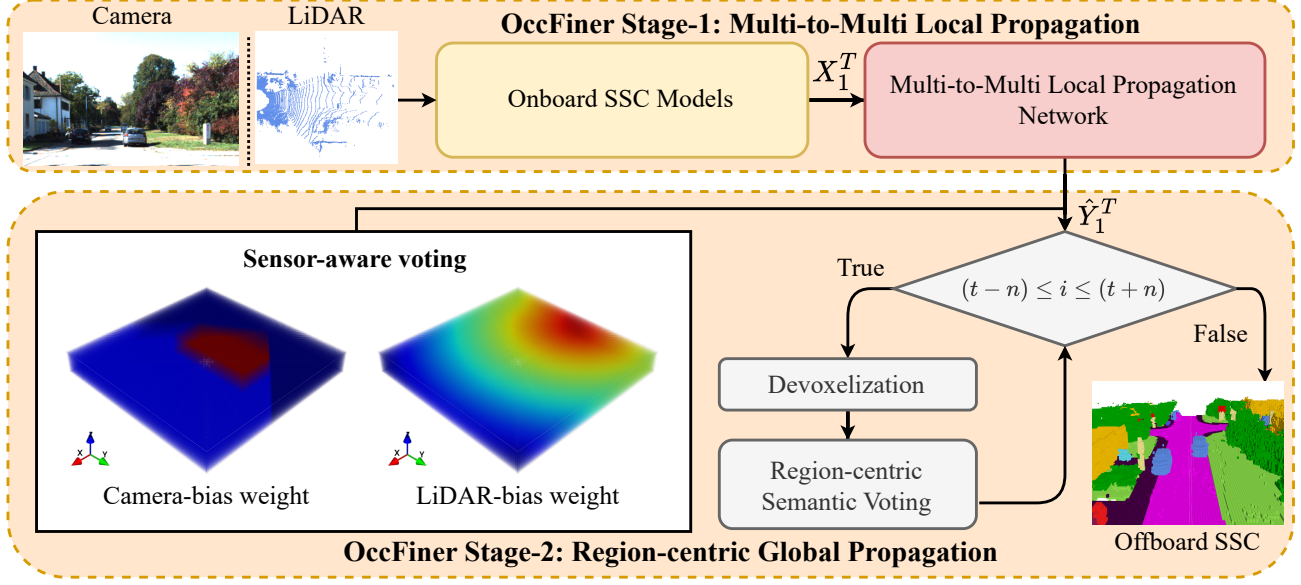


Fig. 4. **Overview of the proposed region-centric global propagation.** Given an arbitrary number of input frames, we leverage multi-view geometry and consider sensor bias to augment long-term SSC consistency and accuracy.

where $Q_z, K_z, V_z \in \mathbb{R}^{W_z \times T \times c_e}$ are respectively reshaped queries, keys, and values. Finally, the output of the entire propagated feature will be gathered:

$$Z_{4d} = \mathcal{P}_z(Z_z) + \mathcal{P}_{bev}(Z_{bev}), \quad (6)$$

where \mathcal{P}_z and \mathcal{P}_{bev} are linear projections. Note that the above formulas omit the head dimension for simplicity. Such a 4D dual-branch design promotes learning coherent spatial-temporal transformations by preserving both BEV information flow and the height dimension information flow along the pillar-shape voxels.

C. Region-centric Global Propagation

In the initial stage, the OccFiner framework engages in multi-to-multi local propagation for offboard SSC (Semantic Scene Completion) refinement. This stage, however, is limited by the input multi-frame window size, leading to a necessity for global propagation across the entire scene sequence. Notably, the local propagation process uniformly enhances SSC accuracy regardless of the various distances, a key aspect of global propagation’s effectiveness. Additionally, OccFiner utilizes relative coordinates in the initial stage, ensuring the implicit alignment of multiple frames and maintaining the contextual integrity of each frame’s semantic content. This approach, which prevents truncation, is pivotal for learning-based error compensation. The subsequent stage involves geometric explicit registration voting, covering the entire scene sequence, and forming a cohesive and hybrid strategy within the OccFiner framework. In the global propagation stage, OccFiner focuses on addressing the measurement limitations of camera and LiDAR sensors and aggregates the independent SSC predictions into a multi-view consistent prediction for each region. OccFiner adeptly integrates sensor-aware weight biases with vanilla registration methods, aligning the refinement process with the unique attributes of each sensor type.

Next, we delve into the details of vanilla registration and enhanced sensor-aware registration.

Vanilla Registration: As illustrated in Fig. 4, it aggregates independent SSC predictions from $2n+1$ frames into a multi-view consistent prediction for each region, where n is the temporal window radius. This involves the aggregation of per-frame semantics and geometry $\{\hat{Y}_i\}_{i=1}^{2n+1}$ into a refined SSC map. For a given target voxel index \mathbf{y} within a 3D region of target \hat{Y}_{tg} , the process starts with devoxelizing the current SSC voxel \hat{Y}_{cur} to derive the semantic point cloud \mathbf{P}_{cur} in the current LiDAR coordinate system:

$$\mathbf{P}_{cur}(x, y, z, c) = \{(o_x + i \cdot dv_x, o_y + j \cdot dv_y, o_z + k \cdot dv_z, c) \mid \hat{Y}_{ijk} = c\}, \quad (7)$$

where the voxel origin is (o_x, o_y, o_z) . dv denotes the voxel size and c represents the semantic classes. This point cloud is then transformed relative to the target LiDAR coordinate system with poses $\{T_{cur}^{tg}\}_{tg-n}^{tg+n}$.

$$\mathbf{P}_{cur}^{tg} = T_{cur}^{tg} \mathbf{P}_{cur}, \quad (8)$$

followed by voxelization and addition in the voting voxel. The final step involves voting for the final semantic voxel output \bar{Y}_{final} :

$$\bar{Y}_{final} = \operatorname{argmax}_c \left(\sum_{cur=tg-n}^{tg+n} \operatorname{Voxelize}(\mathbf{P}_{cur}^{tg}, c) \right), \quad (9)$$

where the argmax function selects the class c with the highest aggregated value in the voting voxel, determining the final semantic voxel.

Incorporating with Sensor Bias: While vanilla registration averages SSC across multiple frames, it overlooks the differential weighting of different locations. To address this, sensor-aware weighting is introduced, tailored to the distinct characteristics of cameras and LiDARs. This approach is informed by

TABLE I

CAMERA-BASED SEMANTIC SCENE COMPLETION RESULTS ON THE SEMANTICKITTI VALIDATION SET [16]. * REPRESENTS THESE METHODS ARE ADAPTED FOR THE RGB INPUTS, WHICH ARE IMPLEMENTED AND REPORTED IN MONOSCENE [1]. † REPRESENTS THE REPRODUCED RESULT FROM [82].

| Method | | | | | | | | | | | | | | | | | | | | IoU | mIoU |
|-------------------------------------|--------------|-----------------|--------------------|---------------|-----------------------|----------------|-------------------|----------------------|---------------|-----------------|------------------|----------------------|------------------|---------------|--------------------|---------------|-----------------|--------------|----------------------|--------------|--------------|
| | car (3.92%) | bicycle (0.03%) | motorcycle (0.03%) | truck (0.16%) | other-vehicle (0.20%) | person (0.07%) | bicyclist (0.07%) | motorcyclist (0.05%) | road (15.30%) | parking (1.12%) | sidewalk (1.13%) | other-ground (0.56%) | building (14.1%) | fence (3.90%) | vegetation (39.3%) | trunk (0.51%) | terrain (9.17%) | pole (0.29%) | traffic-sign (0.08%) | | |
| LMSCNet* [2] | 18.33 | 0.00 | 0.00 | 0.00 | 0.00 | 0.00 | 0.00 | 0.00 | 40.68 | 4.38 | 18.22 | 0.00 | 10.31 | 1.21 | 13.66 | 0.02 | 20.54 | 0.00 | 0.00 | 28.61 | 6.70 |
| 3DSKetch* [83] | 18.59 | 0.00 | 0.00 | 0.00 | 0.00 | 0.00 | 0.00 | 0.00 | 41.32 | 0.00 | 21.63 | 0.00 | 14.81 | 0.73 | 19.09 | 0.00 | 26.40 | 0.00 | 0.00 | 33.30 | 7.50 |
| AICNet* [84] | 14.71 | 0.00 | 0.00 | 4.53 | 0.00 | 0.00 | 0.00 | 0.00 | 43.55 | 11.97 | 20.55 | 0.07 | 12.94 | 2.52 | 15.37 | 2.90 | 28.71 | 0.06 | 0.00 | 29.59 | 8.31 |
| JS3C-Net* [20] | 24.65 | 0.00 | 0.00 | 4.41 | 6.15 | 0.67 | 0.27 | 0.00 | 50.49 | 11.94 | 23.74 | 0.07 | 15.03 | 3.94 | 18.11 | 4.33 | 26.86 | 3.77 | 1.45 | 38.98 | 10.31 |
| OccFormer [3] | 25.09 | 0.81 | 1.19 | 25.53 | 8.52 | 2.78 | 2.82 | 0.00 | 58.85 | 19.61 | 26.88 | 0.31 | 14.40 | 5.61 | 19.63 | 3.93 | 32.62 | 4.26 | 2.86 | 36.50 | 13.46 |
| MonoScene† [1] | 23.26 | 0.61 | 0.45 | 6.98 | 1.48 | 1.86 | 1.20 | 0.00 | 56.52 | 14.27 | 26.72 | 0.46 | 14.09 | 5.84 | 17.89 | 2.81 | 29.64 | 4.14 | 2.25 | 36.86 | 11.08 |
| TPVFormer [82] | 23.81 | 0.36 | 0.05 | 8.08 | 4.35 | 0.51 | 0.89 | 0.00 | 56.50 | 20.60 | 25.87 | 0.85 | 13.88 | 5.94 | 16.92 | 2.26 | 30.38 | 3.14 | 1.52 | 35.61 | 11.36 |
| VoxFormer [4] | 27.01 | 1.05 | 0.47 | 9.90 | 4.64 | 1.51 | 0.85 | 0.00 | 54.67 | 18.55 | 27.35 | 0.41 | 19.65 | 8.52 | 26.18 | 6.58 | 32.39 | 8.69 | 4.71 | 44.16 | 13.33 |
| Average Fusion (Vox) | 30.35 | 0.88 | 0.41 | 12.92 | 3.99 | 1.60 | 0.86 | 0.00 | 57.60 | 18.53 | 29.44 | 0.28 | 21.83 | 10.50 | 29.24 | 7.44 | 34.61 | 9.79 | 5.54 | 46.03 | 14.52 |
| OccFiner (Mono) w.r.t. MonoScene | 29.12 | 0.41 | 1.41 | 21.19 | 7.85 | 3.97 | 2.28 | 0.00 | 56.62 | 19.64 | 27.62 | 1.48 | 15.07 | 7.18 | 20.89 | 3.89 | 31.79 | 3.92 | 2.39 | 37.42 | 13.45 |
| | +5.86 | -0.20 | +0.96 | +14.21 | +6.37 | +2.11 | +1.08 | - | +0.10 | +5.37 | +0.90 | +1.02 | +0.98 | +1.34 | +3.00 | +1.08 | +2.15 | -0.22 | +0.14 | +0.56 | +2.37 |
| OccFiner (TPV) w.r.t. TPVFormer | 29.19 | 0.69 | 0.00 | 22.73 | 7.05 | 0.95 | 1.40 | 0.00 | 57.15 | 22.78 | 28.35 | 7.93 | 15.10 | 6.87 | 19.88 | 3.09 | 31.02 | 3.70 | 1.92 | 36.54 | 13.30 |
| | +5.38 | +0.33 | -0.05 | +14.65 | +2.70 | +0.44 | +0.51 | - | +0.65 | +2.18 | +2.48 | +7.08 | +1.22 | +0.93 | +2.96 | +0.83 | +0.64 | +0.56 | +0.40 | +0.93 | +1.94 |
| OccFiner (Vox) w.r.t. VoxFormer | 36.78 | 1.73 | 0.29 | 32.96 | 5.67 | 4.06 | 1.12 | 0.00 | 66.34 | 27.05 | 35.06 | 0.35 | 25.46 | 11.79 | 32.82 | 9.87 | 40.56 | 8.02 | 3.58 | 47.86 | 18.09 |
| | +9.77 | +0.68 | -0.18 | +22.05 | +1.03 | +2.55 | +0.27 | - | +11.67 | +8.50 | +7.71 | -0.06 | +5.81 | +3.27 | +6.64 | +3.29 | +8.17 | -0.67 | -1.13 | +3.70 | +4.76 |

the measurement characteristics of measurement devices like cameras and LiDARs. Camera systems are constrained by their field of view, with points within the viewing frustum yielding higher accuracy compared to those outside. Additionally, the occlusion of distant points by nearer ones necessitates lower voting weights for the former. Conversely, LiDAR systems exhibit increased sparsity and depth measurement errors at longer distances. Therefore, for cameras, points within the field of view and at closer ranges are given higher voting weights:

$$F_{cam}(x_c, y_c, z_c) = \left(|\theta_{xc}| \leq \frac{fov_h}{2} \right) \wedge \left(|\theta_{yc}| \leq \frac{fov_w}{2} \right) \wedge (z_c > 0), \quad (10)$$

$$W_{cam}(\mathbf{x}) = \begin{cases} w_{high}, & \text{if } (F_{cam} \wedge B)(\mathbf{x}) > 0 \\ w_{med}, & \text{if } [F_{cam}(\mathbf{x}) > 0] \wedge [B(\mathbf{x}) < 0] \\ w_{low}, & \text{otherwise} \end{cases} \quad (11)$$

where (x_c, y_c, z_c) are the voxel indices in the camera coordinate system, fov denotes the field of view of the camera, F_{cam} represents the voxels within the frustum, and B is the bounding box voxel with values being True inside the box and False outside. \mathbf{x} is the vertex and W_{cam} is the final camera voting weight.

While for LiDARs, the voting weight linearly attenuates with increasing distance from the LiDAR center:

$$W_{li}(r) = w_{max} - (w_{max} - w_{min}) \times \frac{r}{R}, \quad (12)$$

where r denotes the radial distance from the origin in the LiDAR coordinate system, R represents the maximum range, and w_{max} and w_{min} correspond to the maximum and minimum weights, respectively. Consequently, the OccFiner framework adopts a hybrid dual-stage strategy: the first stage addresses

onboard model errors, enhancing prediction accuracy regardless of the range, and the second stage adjusts for the physical limitations of cameras and LiDARs, further improving the offboard accuracy.

D. Supervision

Our multi-to-multi local propagation network is trained with the labels from the training set frame-by-frame, while the region-centric global propagation is a learning-free process. The SSC loss \mathcal{L}_{ssc} for network training consists of two parts as below:

$$\mathcal{L}_{ssc} = \mathcal{L}_{ce} + \mathcal{L}_{lovasz}, \quad (13)$$

where \mathcal{L}_{ce} is the cross-entropy loss and \mathcal{L}_{lovasz} is the Lovász loss [85].

IV. EXPERIMENTS

A. Datasets and Implementation Details

SemanticKITTI and SSCBench-KITTI360: The SemanticKITTI dataset [16] is a pivotal SSC benchmark featuring 22 outdoor driving scenarios, segmented into train, validation, and test sets with a 10/1/11 split. The focus is on a specific volume around the vehicle, mapped in $256 \times 256 \times 32$ voxel grids, where each voxel measures $0.2m^3$. SSCBench-KITTI360 [68], derived from KITTI-360 [86], spans $73.7km$ with extensive image and laser scan data, providing diverse geographical coverage and extended sequences. This dataset, sampled to reduce redundancy, offers around $13k$ frames, serving as a vital resource for SSC research.

Training and Optimization: Models are trained for 10 epochs on the SemanticKITTI and 15 on SSCBench-KITTI360, using the Adam optimizer [87] with a learning rate of 0.001. The

TABLE II
 QUANTITATIVE COMPARISON AGAINST THE STATE-OF-THE-ART **LiDAR**-BASED SSC METHODS ON THE SEMANTICKITTI VALIDATION SET. † RESULTS FROM THE OFFICIAL CODE RELEASE.

| Methods | Modality | IoU (%) | | | mIoU (%) | | | Rel. |
|------------------------|----------|--------------|--------------|--------------|--------------|--------------|--------------|---------|
| | | 12.8m | 25.6m | 51.2m | 12.8m | 25.6m | 51.2m | |
| VoxFormer [4] | Camera | 65.38 | 57.70 | 44.16 | 22.13 | 18.58 | 13.33 | - |
| OccFiner (VoxFormer) | Camera | 65.42 | 58.50 | 47.86 | 23.43 | 21.29 | 18.09 | ↑24.59% |
| SSCNet [18] | LiDAR | 50.85 | 52.54 | 44.90 | 17.59 | 17.39 | 14.11 | - |
| OccFiner (SSCNet) | LiDAR | 69.64 | 67.65 | 55.92 | 23.90 | 23.26 | 19.28 | ↑36.64% |
| SSCNet-full [18] | LiDAR | 64.37 | 61.02 | 50.22 | 20.02 | 19.68 | 16.35 | - |
| OccFiner (SSCNet-full) | LiDAR | 65.96 | 64.55 | 54.45 | 23.41 | 23.31 | 19.77 | ↑20.92% |
| LMSCNet [2] | LiDAR | 74.88 | 69.45 | 55.22 | 22.37 | 21.50 | 17.19 | - |
| OccFiner (LMSC) | LiDAR | 75.18 | 69.72 | 57.25 | 24.01 | 23.29 | 19.88 | ↑15.65% |
| SCPNet† [17] | LiDAR | 73.88 | 64.09 | 49.06 | 48.62 | 44.62 | 35.06 | - |
| OccFiner (SCPNet) | LiDAR | 76.44 | 67.33 | 57.19 | 48.70 | 45.90 | 40.26 | ↑14.83% |

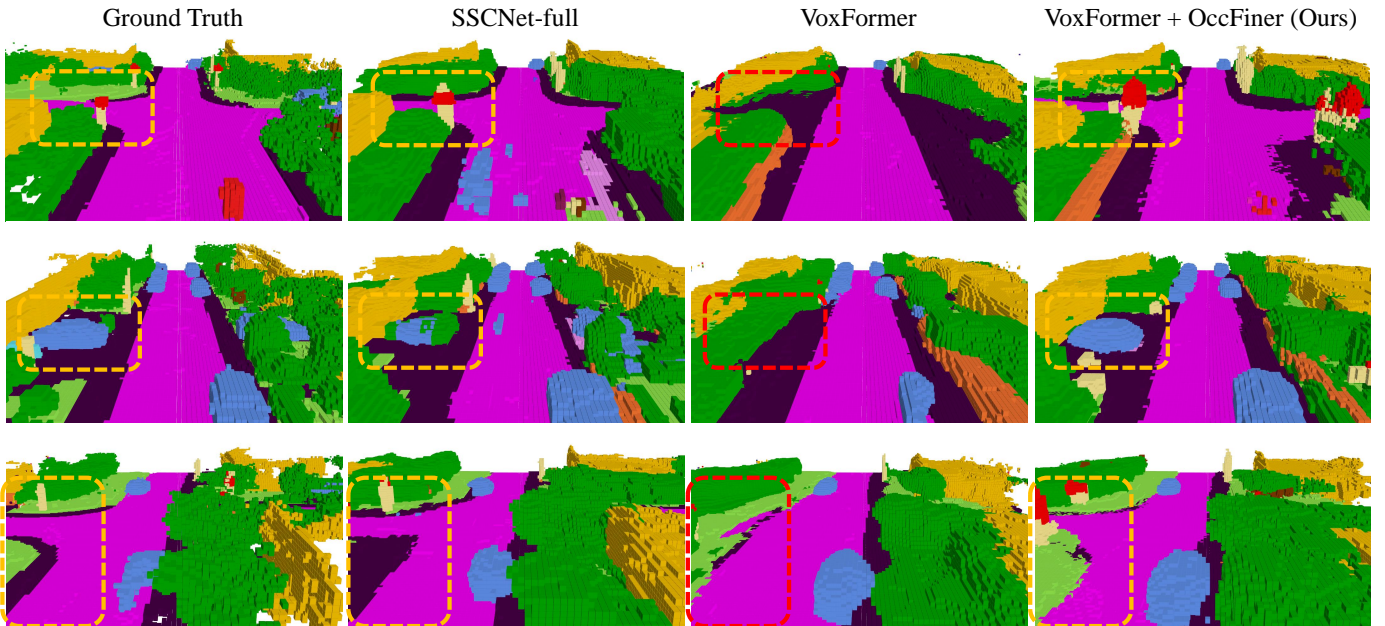


Fig. 5. **Qualitative comparisons.** Our offboard solution effectively fixes critical errors in onboard component [4], such as large areas of *missing road and vehicles*. Moreover, OccFiner elevates the performance of pure visual solutions beyond the classic *LiDAR*-based onboard method SSCNet-full [18].

rate decay is 0.98^{epoch} . Training is performed on 8 RTX 3090 GPUs and includes x-y flipping augmentation in 3D volume space.

Details for Multi-to-Multi Local Propagation Network

In our implementation, the BEV feature and positional encoders are structured as an embedding Linear layer with LayerNorm and four convolutional blocks. Each block uses MaxPool for downsampling by a factor of 2, includes two BEV 3×3 2D convolutions with ReLU activation, and outputs features with a channel of 80. For the DualFlow4D block’s BEV branch, we set the bev patch size at $W_h = 7$, $W_w = 7$, and $T = 6$. The local and distant reference time windows are $T_l = 4$ and $T_r = 2$, respectively, with a reference frame sampling temporal radius of $n = 10$ and a hidden dimension

of $c_e = 256$. The pillar branch of the DualFlow4D block is set at $W_z = 32$ and $T = 6$. Across all experiments, we stack $N = 2$ DualFlow4D Transformer blocks to achieve the desired functionality.

Details for Region-centric Global Propagation For global propagation in each SSC frame, we use a temporal radius of $n = 25$. Camera voting weights are set at $w_{high} = 1$, $w_{med} = 0.1$, and $w_{low} = 0.01$, with a bounding box of $25.6m \times 25.6m \times 6.4m$. For LiDAR, the voting weights range from $w_{max} = 10$ to $w_{min} = 0.1$. We employ vectorization to expedite the global propagation and, due to memory constraints, use single-precision (float) calculations for semantic voxel registration and 8-bit quantization (uint8) in generating city-level global street view maps. In addition,

TABLE III
SEMANTIC SCENE COMPLETION RESULTS ON THE SEMANTICKITTI HIDDEN TEST SET [16]. * REPRESENTS THESE METHODS ARE ADAPTED FOR THE RGB INPUTS, WHICH ARE IMPLEMENTED AND REPORTED IN MONOSCENE [1]. † RESULTS FROM THE OFFICIAL CODE RELEASE.

| Method | Modality | Class (Prevalence) | | | | | | | | | | | | | | | | | IoU | mIoU | | |
|-------------------|----------|--------------------|-----------------|--------------------|---------------|-----------------------|----------------|-------------------|----------------------|---------------|-----------------|-------------------|----------------------|------------------|---------------|--------------------|---------------|-----------------|--------------|--------------|--------------|----------------------|
| | | car (3.92%) | bicycle (0.03%) | motorcycle (0.03%) | truck (0.16%) | other-vehicle (0.20%) | person (0.07%) | bicyclist (0.07%) | motorcyclist (0.06%) | road (15.30%) | parking (1.12%) | sidewalk (11.13%) | other-ground (0.56%) | building (14.1%) | fence (3.90%) | vegetation (39.3%) | trunk (0.51%) | terrain (9.17%) | | | pole (0.29%) | traffic-sign (0.08%) |
| LMSCNet* [2] | Camera | 14.30 | 0.00 | 0.00 | 0.30 | 0.00 | 0.00 | 0.00 | 0.00 | 46.70 | 13.50 | 19.50 | 3.10 | 10.30 | 5.40 | 10.80 | 0.00 | 10.40 | 0.00 | 0.00 | 31.38 | 7.07 |
| 3DSketch* [83] | Camera | 17.10 | 0.00 | 0.00 | 0.00 | 0.00 | 0.00 | 0.00 | 0.00 | 37.70 | 0.00 | 19.80 | 0.00 | 12.10 | 3.40 | 12.10 | 0.00 | 16.10 | 0.00 | 0.00 | 26.85 | 6.23 |
| AICNet* [84] | Camera | 15.30 | 0.00 | 0.00 | 0.70 | 0.00 | 0.00 | 0.00 | 0.00 | 39.30 | 19.80 | 18.30 | 1.60 | 9.60 | 5.00 | 9.60 | 1.90 | 13.50 | 0.10 | 0.00 | 23.93 | 7.09 |
| JS3C-Net* [20] | Camera | 20.10 | 0.00 | 0.00 | 0.80 | 4.10 | 0.00 | 0.20 | 0.20 | 47.30 | 19.90 | 21.70 | 2.80 | 12.70 | 8.70 | 14.20 | 3.10 | 12.40 | 1.90 | 0.30 | 34.00 | 8.97 |
| OccFormer [3] | Camera | 21.60 | 1.50 | 1.70 | 1.20 | 3.20 | 2.20 | 1.10 | 0.20 | 55.90 | 31.50 | 30.30 | 6.50 | 15.70 | 11.90 | 16.80 | 3.90 | 21.30 | 3.80 | 3.70 | 34.53 | 12.32 |
| MonoScene [1] | Camera | 18.80 | 0.50 | 0.70 | 3.30 | 4.40 | 1.00 | 1.40 | 4.40 | 54.70 | 24.80 | 27.10 | 5.70 | 14.40 | 11.10 | 14.90 | 2.40 | 19.50 | 3.30 | 2.10 | 34.16 | 11.08 |
| TPVFormer [82] | Camera | 19.20 | 1.00 | 0.50 | 3.70 | 2.30 | 1.10 | 2.40 | 0.30 | 55.10 | 27.40 | 27.20 | 6.50 | 14.80 | 11.00 | 13.90 | 2.60 | 20.40 | 2.90 | 1.50 | 34.25 | 11.26 |
| VoxFormer [4] | Camera | 21.80 | 0.90 | 1.20 | 5.60 | 2.80 | 1.00 | 1.30 | 0.00 | 54.10 | 24.70 | 27.80 | 9.20 | 23.40 | 14.20 | 24.60 | 9.00 | 23.40 | 6.70 | 6.60 | 43.09 | 13.60 |
| OccFiner (Vox) | Camera | 31.10 | 1.90 | 1.60 | 7.80 | 2.50 | 3.80 | 2.00 | 0.00 | 62.00 | 35.20 | 36.10 | 13.70 | 28.10 | 18.70 | 29.10 | 9.60 | 31.70 | 6.60 | 6.50 | 45.54 | 17.27 |
| w.r.t. VoxFormer | - | +9.30 | +1.00 | +0.40 | +2.20 | -0.30 | +2.80 | +0.70 | - | +7.90 | +10.50 | +8.30 | +4.50 | +4.70 | +4.50 | +4.50 | +0.60 | +8.30 | -0.10 | -0.10 | +2.45 | +3.67 |
| SSCNet-Full [18] | LiDAR | 24.30 | 0.50 | 0.80 | 1.20 | 4.30 | 0.30 | 0.30 | 0.00 | 51.20 | 27.10 | 30.80 | 6.40 | 34.50 | 19.90 | 35.30 | 18.20 | 29.00 | 13.10 | 6.70 | 50.00 | 16.10 |
| ESSCNet [88] | LiDAR | 26.40 | 0.30 | 5.40 | 5.00 | 9.10 | 2.90 | 2.70 | 0.10 | 43.80 | 26.90 | 28.10 | 10.30 | 29.80 | 23.30 | 35.80 | 20.10 | 28.70 | 16.40 | 16.70 | 41.80 | 17.50 |
| LMSCNet [2] | LiDAR | 30.90 | 0.00 | 0.00 | 1.50 | 0.80 | 0.00 | 0.00 | 0.00 | 64.80 | 29.00 | 34.70 | 4.60 | 38.10 | 21.30 | 41.30 | 19.90 | 32.10 | 15.00 | 0.80 | 56.70 | 17.60 |
| SCPNet† [17] | LiDAR | 42.30 | 33.70 | 33.60 | 12.20 | 26.00 | 18.40 | 17.00 | 1.60 | 69.50 | 51.70 | 49.50 | 29.20 | 35.40 | 41.50 | 41.80 | 38.40 | 49.70 | 37.80 | 27.10 | 55.15 | 34.54 |
| OccFiner (SCPNet) | LiDAR | 49.00 | 38.30 | 40.20 | 13.30 | 28.10 | 19.60 | 20.00 | 1.80 | 74.70 | 52.10 | 54.70 | 30.90 | 40.90 | 44.70 | 49.20 | 40.80 | 54.40 | 38.40 | 27.40 | 61.68 | 37.82 |
| w.r.t. SCPNet | - | +6.70 | +4.60 | +6.60 | +1.10 | +2.10 | +1.20 | +3.00 | +0.20 | +5.20 | +0.40 | +5.20 | +1.70 | +5.50 | +3.20 | +7.40 | +2.40 | +4.70 | +0.60 | +0.30 | +6.53 | +3.28 |

TABLE IV
BENCHMARKING RESULTS ON SSCBENCH-KITTI360 [68]. THE DEFAULT EVALUATION RANGE IS $51.2 \times 51.2 \times 6.4m^3$.

| Method | Input | IoU | mIoU | car | bicycle | motorcycle | truck | other-veh. | person | road | parking | sidewalk | other-grnd | building | fence | vegetation | terrain | pole | traf.-sign | other-struct. | other-object |
|------------------|-------|--------------|--------------|--------------|--------------|--------------|--------------|--------------|--------------|--------------|--------------|--------------|--------------|--------------|--------------|--------------|--------------|--------------|--------------|---------------|--------------|
| | | | | car | bicycle | motorcycle | truck | other-veh. | person | road | parking | sidewalk | other-grnd | building | fence | vegetation | terrain | pole | traf.-sign | other-struct. | other-object |
| LMSCNet [2] | L | 47.53 | 13.65 | 20.91 | 0.00 | 0.00 | 0.26 | 0.00 | 0.00 | 62.95 | 13.51 | 33.51 | 0.20 | 43.67 | 0.33 | 40.01 | 26.80 | 0.00 | 0.00 | 3.63 | 0.00 |
| SSCNet [18] | L | 53.58 | 16.95 | 31.95 | 0.00 | 0.17 | 10.29 | 0.58 | 0.07 | 65.70 | 17.33 | 41.24 | 3.22 | 44.41 | 6.77 | 43.72 | 28.87 | 0.78 | 0.75 | 8.60 | 0.67 |
| Voxformer [4] | C | 38.76 | 11.91 | 17.84 | 1.16 | 0.89 | 4.56 | 2.06 | 1.63 | 47.01 | 9.67 | 27.21 | 2.89 | 31.18 | 4.97 | 28.99 | 14.69 | 6.51 | 6.92 | 3.79 | 2.43 |
| MonoScene [1] | C | 37.87 | 12.31 | 19.34 | 0.43 | 0.58 | 8.02 | 2.03 | 0.86 | 48.35 | 11.38 | 28.13 | 3.22 | 32.89 | 3.53 | 26.15 | 16.75 | 6.92 | 5.67 | 4.20 | 3.09 |
| OccFiner (Mono) | C | 38.51 | 13.29 | 20.78 | 1.08 | 1.03 | 9.04 | 3.58 | 1.46 | 53.47 | 12.55 | 31.27 | 4.13 | 33.75 | 4.62 | 26.83 | 18.67 | 5.04 | 4.58 | 4.05 | 3.32 |
| w.r.t. MonoScene | - | +0.64 | +0.98 | +1.44 | +0.65 | +0.45 | +1.02 | +1.55 | +0.60 | +5.12 | +1.17 | +3.14 | +0.91 | +0.86 | +1.09 | +0.68 | +1.92 | -1.88 | -1.09 | -0.15 | +0.23 |

when determining the semantic category of each voxel of the city-level SSC map, we use a three-dimensional sliding window strategy to implement argmax for different map chunks and finally fuse them into a global three-dimensional semantic map to further reduce memory consumption.

B. Comparison with State-of-the-Art

As our work presents the *first* offboard SSC generation, there are no existing competitors to parallel OccFiner’s performance. Additionally, our OccFiner can utilize any off-the-shelf onboard model as its intermediate component.

Quantitatively comparisons. As shown in Tab. I, we use the camera-based SSC algorithm [1], [4], [82] as the onboard component. On the SemanticKITTI validation set [16], OccFiner demonstrates substantial improvements in mIoU accuracy for various algorithms like MonoScene [1], TPVFormer [82], and VoxFormer [4]. The mIoU accuracy is relatively improved by

21.39%, 17.08%, and 35.71%, respectively. Notably, OccFiner (Vox) achieves the new state-of-the-art camera SSC accuracy of 18.09% mIoU. To ensure a meaningful and fair comparison, we also establish an offboard baseline algorithm, “Average Fusion”. It performs region-centric aggregation without learning refinement or considering sensor measurement biases. Despite this, compared to VoxFormer + Average Fusion, our OccFiner (Vox) can still improve SSC quality by a large margin of over 24.59% in mIoU under the long-range setting.

Our exploration extends to validating OccFiner’s versatility across different modalities in offboard SSC generation. As shown in Tab. II, for LiDAR-based SSC models like SSCNet [18], SSCNet-full [18], LMSCNet [2], and SCPNet [17], OccFiner consistently attains relative mIoU improvements of 36.64%, 20.92%, 15.65%, and 14.83%, respectively. This demonstrates its modality-agnostic capability. We observe that the enhancements offered by OccFiner are consistent across

TABLE V
 AUTO-LABELING COMPARISON BETWEEN ONBOARD MODELS TRAINED WITH EITHER TRAINING SET GROUND-TRUTH LABELS (GT-TRAIN) OR AUTO-LABELING MIXED GT-TRAIN + PSEUDO-LABELS (PL) GENERATED BY DIFFERENT SOURCES.

| Label | Source | IoU | mIoU |
|---|----------------------|--------------|--------------|
| GT-Train | Human Labeling | 36.42 | 13.17 |
| GT-Train + PL-Test (SSCNet [18]) | LiDAR Auto-Labeling | 37.07 | 13.63 |
| GT-Train + PL-Test (VoxFormer [4]) | Visual Auto-Labeling | 36.15 | 12.74 |
| GT-Train + PL-Test (VoxFormer [4] + OccFiner) | Visual Auto-Labeling | 37.17 | 13.90 |

TABLE VI
 CITY-LEVEL SEMANTIC SCENE COMPLETION RESULTS ON THE SEMANTICKITTI VALIDATION SET [16]. NOTE WE ONLY COMPARE STATIC CLASSES IN THE GLOBAL MAP COMPARISONS. † RESULTS FROM THE OFFICIAL CODE RELEASE.

| Method | Modality | Class | | | | | | | | | | | IoU | mIoU |
|-------------------------|----------|---------------|-----------------|------------------|----------------------|------------------|---------------|--------------------|---------------|-----------------|--------------|----------------------|--------------|--------------|
| | | road (15.30%) | parking (1.12%) | sidewalk (1.13%) | other-ground (0.56%) | building (14.1%) | fence (3.90%) | vegetation (39.3%) | trunk (0.51%) | terrain (9.17%) | pole (0.29%) | traffic-sign (0.08%) | | |
| SSCNet [18] | LiDAR | 32.78 | 11.88 | 18.00 | 0.00 | 14.58 | 9.17 | 26.78 | 13.48 | 26.56 | 19.88 | 4.70 | 30.06 | 16.16 |
| SSCNet-full [18] | LiDAR | 43.82 | 12.52 | 21.24 | 0.35 | 14.58 | 10.05 | 27.18 | 16.46 | 33.25 | 24.47 | 6.92 | 32.83 | 19.16 |
| LMSCNet [2] | LiDAR | 49.71 | 16.73 | 25.89 | 0.00 | 18.93 | 11.67 | 34.73 | 15.68 | 35.16 | 26.81 | 0.69 | 41.66 | 21.45 |
| SCPNet† [17] | LiDAR | 74.81 | 52.43 | 50.80 | 7.85 | 38.91 | 28.99 | 45.30 | 36.27 | 54.86 | 41.33 | 25.59 | 59.39 | 41.55 |
| OccFiner (SCP) | LiDAR | 72.76 | 51.56 | 50.57 | 10.03 | 41.40 | 30.61 | 47.09 | 39.86 | 55.11 | 42.64 | 26.76 | 60.16 | 42.58 |
| <i>w.r.t. SCPNet</i> | - | -2.05 | -0.87 | -0.23 | +2.18 | +2.49 | +1.62 | +1.79 | +3.59 | +0.25 | +1.31 | +1.17 | +0.77 | +1.03 |
| MonoScene [1] | Camera | 47.07 | 10.04 | 15.32 | 0.58 | 10.39 | 9.74 | 17.41 | 5.13 | 25.44 | 7.31 | 5.37 | 29.75 | 13.98 |
| OccFormer [3] | Camera | 46.70 | 17.90 | 14.77 | 0.95 | 9.17 | 7.31 | 20.40 | 5.93 | 24.64 | 6.87 | 5.77 | 27.63 | 14.58 |
| TPVFormer [82] | Camera | 43.49 | 15.28 | 13.46 | 0.51 | 8.91 | 8.74 | 17.28 | 4.86 | 24.53 | 6.34 | 4.23 | 26.61 | 13.42 |
| VoxFormer [4] | Camera | 42.22 | 12.48 | 15.16 | 0.36 | 13.04 | 10.12 | 22.21 | 10.02 | 25.63 | 12.36 | 6.71 | 32.66 | 15.48 |
| OccFiner (Vox) | Camera | 47.44 | 16.22 | 21.04 | 0.83 | 13.29 | 9.96 | 27.17 | 10.62 | 24.75 | 10.33 | 5.19 | 33.59 | 16.99 |
| <i>w.r.t. VoxFormer</i> | - | +5.22 | +3.74 | +5.88 | +0.47 | +0.25 | -0.16 | +4.96 | +0.60 | -0.88 | -2.03 | -1.52 | +0.93 | +1.51 |

varying distances. This improvement is not only confined to long distances and low-accuracy scenarios but also extends to challenging high-accuracy short-range as well, indicating a robust and versatile perception of the framework. Remarkably, the accuracy of OccFiner (VoxFormer) even surpasses onboard LiDAR-based SSC models including SSCNet, SSCNet-full, and LMSCNet. This is the first time that the camera-based SSC model surpasses the LiDAR-based SSC model in accuracy. Compared with the onboard LiDAR-based LMSCNet, the camera-based OccFiner (VoxFormer) achieves a relative mIoU improvement of 5.24%. This proves that OccFiner unleashes the potential of the camera-based SSC applications. This breakthrough in the camera-based versus LiDAR-based SSC model signifies a crucial advancement for autonomous driving, notably in the realms of pure visual SSC data closure and auto-labeling.

As shown in Tab. III, in the results submitted for the hidden test set of SemanticKITTI [16], OccFiner showcases remarkable performance. The OccFiner (Vox) and OccFiner (SCP-Net) establish new state-of-the-art accuracy for camera-based

and LiDAR-based SSC respectively. They deliver significant relative mIoU improvements compared to the best-published results of 26.99% and 9.50%, respectively. The OccFiner (Vox) consistently surpasses the SSCNet-full [18]. This further demonstrates the efficacy and advancement of the OccFiner framework.

The effectiveness of OccFiner is also assessed on the SSCBench-KITTI360 dataset [68]. As shown in Tab. IV, OccFiner (Mono) demonstrates notable performance, achieving a relative improvement in mIoU of 7.96% compared to MonoScene [1]. This underscores OccFiner’s capability to enhance SSC accuracy across diverse datasets.

Qualitative comparisons. As shown in Fig. 5, our offboard solution, OccFiner, effectively corrects major onboard errors, notably in resolving extensive missing road and vehicle voxels. Furthermore, OccFiner enhances the effectiveness of purely visual approaches, surpassing the traditional *LiDAR-based* onboard method SSCNet-full [18] in performance, indicating its potential to advance the field of autonomous navigation with pure visual solution.

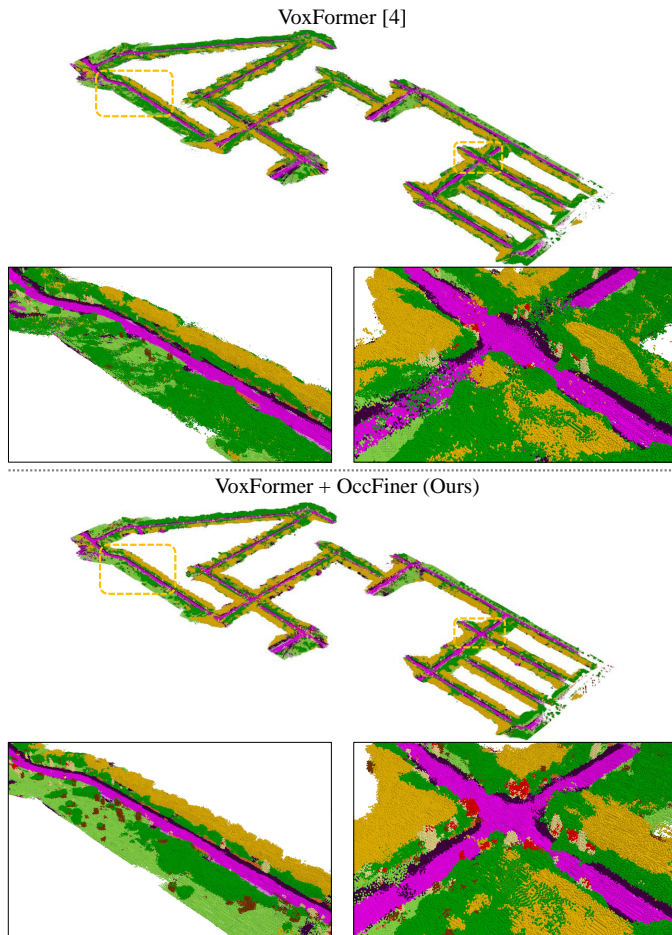


Fig. 6. **City-level semantic scene completion.** The city-scale scene is expanded from the original size of $256 \times 256 \times 32$ to $2205 \times 4296 \times 261$.

Latency. The online component VoxFormer [4] exhibits a latency of 1.52 s/frame on a single NVIDIA RTX 3090 with single-precision computation. In contrast, the multi-to-multi local propagation network of OccFiner incurs a computational delay of 0.027 s/frame on the same device. Furthermore, the region-centric global propagation on an Intel i9-13980HX CPU has a computational delay of 5.96 s/frame.

C. Auto-labeling Experiments

The aforementioned results highlight OccFiner’s ability to generate superior Semantic Scene Completion (SSC) labels, indicating its promise as an offboard solution for automatic SSC labeling and data closure, particularly for augmenting manual labeling in novel scenarios using pure vision-based solution. To evaluate OccFiner’s label quality further, we conduct auto-labeling experiments on SemanticKITTI [16], detailed in Table V, which simulate a real-world data loop. Utilizing manually annotated labels as a base, we enrich new scenes from the test sequences with pseudo-labels created by the pure-vision VoxFormer + OccFiner. Comparing training results of an onboard visual SSC model [3] *from scratch* under different labeling conditions, we find that directly using VoxFormer for ‘Visual Auto-Labeling’ cannot achieve data closure, and the IoU and mIoU of the onboard model dropped

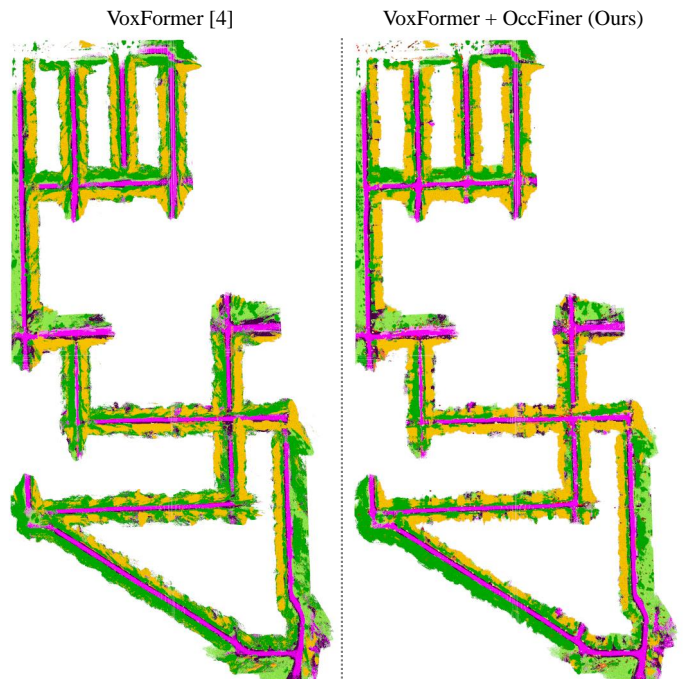


Fig. 7. **City-level semantic scene completion in BEV.** Only static classes are considered. Our proposed OccFiner preserves more high-quality details and reduces camera frustum artifacts.

by 0.27% and 0.43%, respectively. Meanwhile, ‘LiDAR Auto-Labeling’ based on SSCNet [18] can improve the accuracy of the visual onboard model by 0.46%. Keeping hyperparameters and model structure consistent, we find that OccFiner’s ‘Visual Auto-Labeling’ outperforms ‘Human Labeling’ alone. Consequently, the onboard model’s IoU on the validation set improved by 0.75%, with a corresponding large increase of 0.73% in mIoU. When compared under varied labeling conditions, OccFiner’s visual auto-labeling significantly improves onboard model performance, demonstrating a notable advantage over both pure human labeling and even LiDAR-based auto-labeling. This underscores our method’s ability to effectively close data loops in SSC applications using high-quality, visually-derived labels.

D. City-level SSC Map Comparisons

Previous works usually focus on local 3D semantic occupancy, *i.e.*, onboard perception centered on a single vehicle. However, for multi-vehicle collaborative sensing, task scheduling, and traffic control, establishing a city-level SSC map is of great significance. Therefore, we propose to fuse local SSC predictions using relative poses to further explore the effectiveness of OccFiner in establishing visually derived city-level SSC results. In the global map, we only consider static rigid targets of the scene, since dynamic targets are not among the usual properties of maps.

Quantitatively Comparisons As shown in Table VI, we benchmark the mainstream LiDAR- and camera-based SSC methods, and explore OccFiner + VoxFormer to establish an offboard city-level SSC Map. Experimental results show that the accuracy of the LiDAR-based SSC method is consistently

TABLE VII
 ABLATION EXPERIMENTS. SETTINGS USED IN OUR FINAL FRAMEWORK ARE UNDERLINED. SEE SEC. IV-E FOR DETAILS.

| Experiment | Method | SemanticKITTI (val) | | | #Parameters |
|--|---|-----------------------|-----------------------|-----------------------|--------------------------------|
| | | Near | Middle | Far | |
| <i>Reference Model</i> (VoxFormer [4]), Training: 10 Epoch (SemanticKITTI [16]). | | | | | |
| Onboard Model | VoxFormer [4] | 22.13 | 18.58 | 13.33 | 551M |
| DualFlow4D Transformer | <i>w/o</i> <u>with</u> | 21.71 23.29 | 19.23 20.25 | 13.96 14.52 | +0.83M +4.51M |
| Temporal Embedding | Embedding <u>Not Embedding</u> | 23.24 23.29 | 20.21 20.25 | 14.50 14.52 | +4.90M +4.51M |
| Spatial Embedding | Not Embedding <u>Embedding</u> | 23.14 23.29 | 19.95 20.25 | 14.40 14.52 | +4.12M +4.51M |
| Reference Frame | <i>w/o</i> <u>with</u> | 22.99 23.29 | 20.04 20.25 | 14.30 14.52 | +4.51M +4.51M |
| <i>Reference Model</i> (VoxFormer [4]), Training: 10 Epoch (SemanticKITTI [16]) → Global Prop. | | | | | |
| Offboard Baseline (Average Fusion) | VoxFormer [4] + Vanilla Registration OccFiner Stage 1 + Vanilla Registration | 21.18 22.60 | 18.36 20.19 | 14.52 16.11 | 551M +4.51M |
| Learning Refine | <i>w/o</i> <u>with</u> | 21.48 23.43 | 18.97 21.29 | 16.05 18.09 | <i>n.a.</i> +4.51M |
| Frustum Weighting | <i>w/o</i> <u>with</u> | 23.09 23.43 | 20.80 21.29 | 17.63 18.09 | +4.51M +4.51M |
| Distance-aware Weighting | <i>w/o</i> <u>with</u> | 23.14 23.43 | 20.92 21.29 | 17.34 18.09 | +4.51M +4.51M |
| Temporal Input | (-5, 5) | 23.41 | 21.11 | 16.25 | +4.51M |
| | (-10, 10) | 23.45 | 21.29 | 17.65 | +4.51M |
| | (-15, 15) | 23.43 | 21.28 | 18.00 | +4.51M |
| | (-20, 20) | 23.43 | 21.28 | 18.05 | +4.51M |
| | (-25, 25) | 23.43 | 21.29 | 18.09 | +4.51M |
| | (-30, 30) | 23.43 | 21.29 | 18.08 | +4.51M |

ahead of the camera-based method in city-level SSC maps. It is worth noting that OccFiner further improves the accuracy of both LiDAR- and camera-based city-level SSC maps. Compared with the onboard component [4], the geometric IoU of OccFiner (Vox) increased by 0.93%, and the semantic mIoU improved by 1.51%. It even exceeds the LiDAR-based SSCNet-full [18] by 0.76% in geometric accuracy and surpasses the LiDAR-based SSCNet [18] by 0.83% in semantic accuracy. This once again proves that the proposed OccFiner framework can effectively unleash the potential of purely visual SSC perception solutions.

Qualitatively Comparisons We visualize the validation sequence of SemanticKITTI [16] to evaluate the quality of city-level semantic scene completion (SSC) maps. The spatial resolution of the original single-frame local occupancy is $256 \times 256 \times 32$. After splicing and voting using relative pose registration, the spatial resolution of the global occupancy map is $2205 \times 4296 \times 261$, covering a spatial range of $441 \times 859.2 \times 52.2 m^3$. As illustrated in Fig. 6, directly using the outputs of the visual SSC algorithm (VoxFormer [4]) for global registration, despite their large onboard errors, leads to artifacts on key road surfaces. The implementation of OccFiner significantly reduces these errors, thereby enhancing the quality of the city-level SSC maps. Additionally, Fig. 7 presents the global map visualized from a bird’s-eye-view (BEV) perspective. The VoxFormer [4] results exhibit notable

radial artifacts, attributed to the limited viewing angle of the camera’s view frustum. In contrast, OccFiner’s region-centric global propagation successfully compensates for the camera’s measurement limitations, effectively eliminating these radial artifacts.

E. Ablation Studies

The efficacy of each module in the offboard OccFiner framework is quantified through ablation studies detailed in Tab. VII. Using VoxFormer [4] as the onboard component, we evaluate mIoU accuracy across different distances.

Multi-to-Multi Local Propagation Network. 1) DualFlow4D Transformer. We validate the critical role of the 4D Transformer for local SSC feature propagation, evidenced by a 0.56% drop in mIoU upon its removal. 2) Temporal Embedding, however, did not positively impact accuracy. 3) Spatial Embedding. The result highlights the importance of spatial embedding and the introduction of a long-distance reference frame in the multi-to-multi paradigm, improving accuracy by 0.12%. 4) Reference Frame. OccFiner introduces a long-distance reference frame in addition to the local clip, which further improves the accuracy by 0.22%. It proves the positive effect of long-term geometric and semantic cues on error compensation. 5) Overall, OccFiner’s first stage, while adding few model parameters (4.51M vs. 551M), effectively compensates for onboard model errors and propagates high-

TABLE VIII
PERFORMANCE OF DIRECTLY USING MULTI-TO-MULTI PROPAGATION NETWORK WITH DIFFERENT TIME WINDOW.

| Dataset | Input | Time Window | mIoU |
|---------------|-------------|-------------|--------------|
| SemanticKITTI | LiDAR Scans | 1 | 17.99 |
| | | 2 | 19.10 |
| | | 4 | 19.98 |
| | | 6 | 20.68 |

confidence features, boosting mIoU from 13.33% to 14.52%, and uniformly improves mIoU across various distances. This is critical for the next global propagation stage. In addition, the local propagation network can also be directly used for LiDAR-based SSC prediction. We add the SSC accuracy of the base model under various time window settings. As shown in Tab. VIII, the accuracy consistently improves with an increase in the time window, while keeping the model structure unchanged. This further underscores the effectiveness and rational design of the base model structure.

Region-centric Global Propagation. 1) Average Fusion. Average fusion applied as a baseline to the onboard model yielded only a modest mIoU improvement at ‘far’, indicating limitations at near and middle distances with 0.95% and 0.22% mIoU drop, respectively. 2) Learning Refine. Removing the local propagation network resulted in a significant drop in mIoU by 2.04%, highlighting the critical role of first-stage error compensation in enhancing global propagation accuracy across various distances. 3) Sensor Bias. the frustum weighting and distance-aware weighting adjustments are shown to be vital, with their removal leading to noticeable accuracy drops. This underscores the importance of considering the camera field of view and depth uncertainties in long-distance measurements. 4) Temporal Input. The optimal number of frames for global propagation is identified around $(-25, 25)$, with more frames offering no additional benefit. 5) Overall, learning-free global propagation significantly improves the accuracy of long-distance prediction. Compared with ‘OccFiner Stage 1 + Vanilla Registration’, OccFiner’s region-centric global propagation further improving the accuracy across different distances by 0.83%, 1.10%, and 1.98%.

The proposed Occfiner, as the first *offboard* occupancy approach, integrating both local and global propagation techniques, not only demonstrates significant improvements in predictive accuracy but also establishes a robust framework for achieving data loop-closure in intelligent transportation systems. By addressing onboard model deficiencies and enhancing error compensation through offboard processing, our methodology lays a solid foundation for future advancements in self-evolving 3D scene understanding technology, promoting safer and more reliable navigation.

V. CONCLUSIONS AND DISCUSSION

In addressing the challenges of inferior performance and data loop-closure in vision-based SSC, we introduce OccFiner, the first offboard SSC setup designed to enhance the reliability of onboard models. By removing computational constraints, OccFiner reasons with all frames together to build multi-view consistent SSC predictions. It employs a hybrid propagation

strategy: compensating for onboard model errors and propagating semantic and geometric cues locally, while managing sensor bias and long-term information aggregation globally. Our experiments validate OccFiner’s versatility across various onboard models and its ability to significantly elevate SSC quality, setting new benchmarks on SemanticKITTI for both vision- and LiDAR-based algorithms. Integrating data into offboard occupancy systems successfully addresses model deficiencies, achieves data loop-closure, and enables system self-evolution. This approach also solves the distribution shift between training and deployment, allowing for scalable, cost-effective improvements in the accurate reconstruction of 3D scenes. We hope that our framework will augment onboard SSC algorithms and inspire future offboard research, advancing autonomous driving technology by reducing manual annotation efforts and improving large-scale 3D scene understanding.

Limitations. Our offboard framework, OccFiner, achieves notable results but requires individual retraining for each onboard model. This process is tailored to address the specific errors of each onboard model, with its effectiveness partly dependent on the scene’s characteristics. Additionally, there is substantial scope for improving offboard SSC accuracy in comparison to the ground truth.

Broader impact, Ethics. While OccFiner improves 3D scene understanding, potential inaccuracies in its predictions could have serious implications, especially in critical applications like autonomous driving. It is crucial that such technologies be complemented by additional safety measures to mitigate risks associated with these inevitable errors.

REFERENCES

- [1] A.-Q. Cao and R. de Charette, “MonoScene: Monocular 3D semantic scene completion,” in *CVPR*, 2022.
- [2] L. Roldao, R. de Charette, and A. Verroust-Blondet, “LMSCNet: Lightweight multiscale 3D semantic completion,” in *3DV*, 2020.
- [3] Y. Zhang, Z. Zhu, and D. Du, “OccFormer: Dual-path transformer for vision-based 3D semantic occupancy prediction,” *arXiv preprint arXiv:2304.05316*, 2023.
- [4] Y. Li, Z. Yu, C. Choy, C. Xiao, J. M. Alvarez, S. Fidler, C. Feng, and A. Anandkumar, “VoxFormer: Sparse voxel transformer for camera-based 3D semantic scene completion,” in *CVPR*, 2023.
- [5] H. Xiao, H. Xu, W. Kang, and Y. Li, “Instance-aware monocular 3D semantic scene completion,” *IEEE Transactions on Intelligent Transportation Systems*, 2024.
- [6] I. Shepel, V. Adeshkin, I. Belkin, and D. A. Yudin, “Occupancy grid generation with dynamic obstacle segmentation in stereo images,” *IEEE Transactions on Intelligent Transportation Systems*, 2022.
- [7] C. Robbiano, E. K. Chong, M. R. Azimi-Sadjadi, L. L. Scharf, and A. Pezeshki, “Bayesian learning of occupancy grids,” *IEEE Transactions on Intelligent Transportation Systems*, 2022.
- [8] J. Li, H. Qu, and L. You, “An integrated approach for the near real-time parking occupancy prediction,” *IEEE Transactions on Intelligent Transportation Systems*, 2023.
- [9] X. Li, Z. Wang, Y. Huang, and H. Chen, “A survey on self-evolving autonomous driving: A perspective on data closed-loop technology,” *IEEE Transactions on Intelligent Vehicles*, 2023.
- [10] C. Zhang, R. Guo, W. Zeng, Y. Xiong, B. Dai, R. Hu, M. Ren, and R. Urtasun, “Rethinking closed-loop training for autonomous driving,” in *ECCV*, 2022.
- [11] L. Li, W. Shao, W. Dong, Y. Tian, K. Yang, and W. Zhang, “Data-centric evolution in autonomous driving: A comprehensive survey of big data system, data mining, and closed-loop technologies,” *arXiv preprint arXiv:2401.12888*, 2024.

- [12] C. R. Qi, Y. Zhou, M. Najibi, P. Sun, K. Vo, B. Deng, and D. Anguelov, "Offboard 3D object detection from point cloud sequences," in *CVPR*, 2021.
- [13] B. Yang, M. Bai, M. Liang, W. Zeng, and R. Urtasun, "Auto4D: Learning to label 4D objects from sequential point clouds," *arXiv preprint arXiv:2101.06586*, 2021.
- [14] L. Fan, Y. Yang, Y. Mao, F. Wang, Y. Chen, N. Wang, and Z. Zhang, "Once detected, never lost: Surpassing human performance in offline LiDAR based 3D object detection," *arXiv preprint arXiv:2304.12315*, 2023.
- [15] T. Ma, X. Yang, H. Zhou, X. Li, B. Shi, J. Liu, Y. Yang, Z. Liu, L. He, Y. Qiao, Y. Li, and H. Li, "DetZero: Rethinking offboard 3D object detection with long-term sequential point clouds," in *ICCV*, 2023.
- [16] J. Behley, M. Garbade, A. Milioto, J. Quenzel, S. Behnke, C. Stachniss, and J. Gall, "SemanticKITTI: A dataset for semantic scene understanding of LiDAR sequences," in *ICCV*, 2019.
- [17] Z. Xia, Y. Liu, X. Li, X. Zhu, Y. Ma, Y. Li, Y. Hou, and Y. Qiao, "SCPNet: Semantic scene completion on point cloud," in *CVPR*, 2023.
- [18] S. Song, F. Yu, A. Zeng, A. X. Chang, M. Savva, and T. Funkhouser, "Semantic scene completion from a single depth image," in *CVPR*, 2017.
- [19] C. B. Rist, D. Emmerichs, M. Enzweiler, and D. M. Gavrila, "Semantic scene completion using local deep implicit functions on LiDAR data," *IEEE Transactions on Pattern Analysis and Machine Intelligence*, 2022.
- [20] X. Yan, J. Gao, J. Li, R. Zhang, Z. Li, R. Huang, and S. Cui, "Sparse single sweep LiDAR point cloud segmentation via learning contextual shape priors from scene completion," in *AAAI*, 2021.
- [21] R. Cheng, C. Agia, Y. Ren, X. Li, and L. Bingbing, "S3CNet: A sparse semantic scene completion network for LiDAR point clouds," in *CoRL*, 2021.
- [22] X. Yang, H. Zou, X. Kong, T. Huang, Y. Liu, W. Li, F. Wen, and H. Zhang, "Semantic segmentation-assisted scene completion for LiDAR point clouds," in *IROS*, 2021.
- [23] S. Zuo, W. Zheng, Y. Huang, J. Zhou, and J. Lu, "PointOcc: Cylindrical tri-perspective view for point-based 3D semantic occupancy prediction," *arXiv preprint arXiv:2308.16896*, 2023.
- [24] X. Yan, R. Chen, B. Zhang, J. Yuan, X. Cai, B. Shi, W. Shao, J. Yan, P. Luo, and Y. Qiao, "SPOT: Scalable 3D pre-training via occupancy prediction for autonomous driving," *arXiv preprint arXiv:2309.10527*, 2023.
- [25] S. Silva, S. B. Wannigama, R. Ragel, and G. Jayatilaka, "S2TPVFormer: Spatio-temporal tri-perspective view for temporally coherent 3D semantic occupancy prediction," *arXiv preprint arXiv:2401.13785*, 2024.
- [26] Q. Ma, X. Tan, Y. Qu, L. Ma, Z. Zhang, and Y. Xie, "COTR: Compact occupancy transformer for vision-based 3D occupancy prediction," *arXiv preprint arXiv:2312.01919*, 2023.
- [27] J. Mei, Y. Yang, M. Wang, J. Zhu, X. Zhao, J. Ra, L. Li, and Y. Liu, "Camera-based 3D semantic scene completion with sparse guidance network," *arXiv preprint arXiv:2312.05752*, 2023.
- [28] Y. Wang, Y. Chen, X. Liao, L. Fan, and Z. Zhang, "PanoOcc: Unified occupancy representation for camera-based 3D panoptic segmentation," in *CVPR*, 2024.
- [29] C. Lyu, S. Guo, B. Zhou, H. Xiong, and H. Zhou, "3DOPFormer: 3D occupancy perception from multi-camera images with directional and distance enhancement," *IEEE Transactions on Intelligent Vehicles*, 2023.
- [30] Y. Wei, L. Zhao, W. Zheng, Z. Zhu, J. Zhou, and J. Lu, "SurroundOcc: Multi-camera 3D occupancy prediction for autonomous driving," in *ICCV*, 2023.
- [31] J. Ma, X. Chen, J. Huang, J. Xu, Z. Luo, J. Xu, W. Gu, R. Ai, and H. Wang, "Cam4DOcc: Benchmark for camera-only 4D occupancy forecasting in autonomous driving applications," in *CVPR*, 2024.
- [32] Y. Lu, X. Zhu, T. Wang, and Y. Ma, "OctreeOcc: Efficient and multi-granularity occupancy prediction using octree queries," *arXiv preprint arXiv:2312.03774*, 2023.
- [33] H. Jiang, T. Cheng, N. Gao, H. Zhang, W. Liu, and X. Wang, "Symphonize 3D semantic scene completion with contextual instance queries," in *CVPR*, 2024.
- [34] Z. Yu, C. Shu, J. Deng, K. Lu, Z. Liu, J. Yu, D. Yang, H. Li, and Y. Chen, "FlashOcc: Fast and memory-efficient occupancy prediction via channel-to-height plugin," *arXiv preprint arXiv:2311.12058*, 2023.
- [35] Z. Li, Z. Yu, D. Austin, M. Fang, S. Lan, J. Kautz, and J. M. Alvarez, "FB-OCC: 3D occupancy prediction based on forward-backward view transformation," *arXiv preprint arXiv:2307.01492*, 2023.
- [36] J. Hou, X. Li, W. Guan, G. Zhang, D. Feng, Y. Du, X. Xue, and J. Pu, "FastOcc: Accelerating 3D occupancy prediction by fusing the 2D bird's-eye view and perspective view," in *ICRA*, 2024.
- [37] W. Zheng, W. Chen, Y. Huang, B. Zhang, Y. Duan, and J. Lu, "OccWorld: Learning a 3D occupancy world model for autonomous driving," *arXiv preprint arXiv:2311.16038*, 2023.
- [38] Y. Jia, J. He, R. Chen, F. Zhao, and H. Luo, "OccupancyDETR: Making semantic scene completion as straightforward as object detection," *arXiv preprint arXiv:2309.08504*, 2023.
- [39] W. Tong, C. Sima, T. Wang, L. Chen, S. Wu, H. Deng, Y. Gu, L. Lu, P. Luo, D. Lin, and H. Li, "Scene as occupancy," in *ICCV*, 2023.
- [40] L. Peng, J. Xu, H. Cheng, Z. Yang, X. Wu, W. Qian, W. Wang, B. Wu, and D. Cai, "Learning occupancy for monocular 3D object detection," *arXiv preprint arXiv:2305.15694*, 2023.
- [41] J. Xu, L. Peng, H. Cheng, L. Xia, Q. Zhou, D. Deng, W. Qian, W. Wang, and D. Cai, "Regulating intermediate 3D features for vision-centric autonomous driving," in *AAAI*, 2024.
- [42] Y. Hong, Q. Liu, H. Cheng, D. Ma, H. Dai, Y. Wang, G. Cao, and Y. Ding, "UniVision: A unified framework for vision-centric 3D perception," *arXiv preprint arXiv:2401.06994*, 2024.
- [43] Q. Zhou, J. Cao, H. Leng, Y. Yin, Y. Kun, and R. Zimmermann, "SOGDet: Semantic-occupancy guided multi-view 3D object detection," in *AAAI*, 2024.
- [44] C. Min, L. Xiao, D. Zhao, Y. Nie, and B. Dai, "Multi-camera unified pre-training via 3D scene reconstruction," *IEEE Robotics and Automation Letters*, 2024.
- [45] B. Li, Y. Sun, Z. Liang, D. Du, Z. Zhang, X. Wang, Y. Wang, X. Jin, and W. Zeng, "Bridging stereo geometry and BEV representation with reliable mutual interaction for semantic scene completion," *arXiv preprint arXiv:2303.13959*, 2023.
- [46] J. Yao and J. Zhang, "DepthSSC: Depth-spatial alignment and dynamic voxel resolution for monocular 3D semantic scene completion," *arXiv preprint arXiv:2311.17084*, 2023.
- [47] H. Zhang, X. Yan, D. Bai, J. Gao, P. Wang, B. Liu, S. Cui, and Z. Li, "RadOcc: Learning cross-modality occupancy knowledge through rendering assisted distillation," in *AAAI*, 2024.
- [48] M. Pan, J. Liu, R. Zhang, P. Huang, X. Li, L. Liu, and S. Zhang, "RenderOcc: Vision-centric 3D occupancy prediction with 2D rendering supervision," *arXiv preprint arXiv:2309.09502*, 2023.
- [49] R. Miao, W. Liu, M. Chen, Z. Gong, W. Xu, C. Hu, and S. Zhou, "OccDepth: A depth-aware method for 3D semantic scene completion," *arXiv preprint arXiv:2302.13540*, 2023.
- [50] Z. Ming, J. S. Berrio, M. Shan, and S. Worrall, "InverseMatrixVT3D: An efficient projection matrix-based approach for 3D occupancy prediction," *arXiv preprint arXiv:2401.12422*, 2024.
- [51] H. Liu, H. Wang, Y. Chen, Z. Yang, J. Zeng, L. Chen, and L. Wang, "Fully sparse 3D panoptic occupancy prediction," *arXiv preprint arXiv:2312.17118*, 2023.
- [52] Z. Ming, J. S. Berrio, M. Shan, and S. Worrall, "OccFusion: A straightforward and effective multi-sensor fusion framework for 3D occupancy prediction," *arXiv preprint arXiv:2403.01644*, 2024.
- [53] A. Hayler, F. Wimbauer, D. Muhle, C. Rupprecht, and D. Cremers, "S4C: Self-supervised semantic scene completion with neural fields," *arXiv preprint arXiv:2310.07522*, 2023.
- [54] C. Zhang, J. Yan, Y. Wei, J. Li, L. Liu, Y. Tang, Y. Duan, and J. Lu, "OccNeRF: Self-supervised multi-camera occupancy prediction with neural radiance fields," *arXiv preprint arXiv:2312.09243*, 2023.
- [55] C. Min, L. Xiao, D. Zhao, Y. Nie, and B. Dai, "Occupancy-MAE: Self-supervised pre-training large-scale LiDAR point clouds with masked occupancy autoencoders," *IEEE Transactions on Intelligent Vehicles*, 2023.
- [56] Y. Huang, W. Zheng, B. Zhang, J. Zhou, and J. Lu, "SelfOcc: Self-Supervised vision-based 3D occupancy prediction," *arXiv preprint arXiv:2311.12754*, 2023.
- [57] S. Boeder, F. Gigengack, and B. Risse, "OccFlowNet: Towards self-supervised occupancy estimation via differentiable rendering and occupancy flow," *arXiv preprint arXiv:2402.12792*, 2024.
- [58] A. Vobecky, O. Siméoni, D. Hurych, S. Gidaris, A. Bursuc, P. Pérez, and J. Sivic, "POP-3D: Open-vocabulary 3D occupancy prediction from images," in *NeurIPS*, 2023.
- [59] Z. Tan, Z. Dong, C. Zhang, W. Zhang, H. Ji, and H. Li, "OVO: Open-vocabulary occupancy," *arXiv preprint arXiv:2305.16133*, 2023.
- [60] K. Peng, J. Fei, K. Yang, A. Roitberg, J. Zhang, F. Bieder, P. Heidenreich, C. Stiller, and R. Stiefelhagen, "MASS: Multi-attentional semantic segmentation of LiDAR data for dense top-view understanding," *IEEE Transactions on Intelligent Transportation Systems*, 2022.
- [61] S. Gu, J. Lu, J. Yang, C.-Z. Xu, and H. Kong, "Dense top-view semantic completion with sparse guidance and online distillation," *IEEE Transactions on Intelligent Vehicles*, 2023.

- [62] J. Lu, S. Gu, C.-Z. Xu, and H. Kong, "A cylindrical convolution network for dense top-view semantic segmentation with LiDAR point clouds," in *ACCV*, 2022.
- [63] Y. Li, J. Zhang, D. Ma, Y. Wang, and C. Feng, "Multi-robot scene completion: Towards task-agnostic collaborative perception," in *CoRL*, 2023.
- [64] Y. Zhang, J. Li, K. Luo, Y. Yang, J. Han, N. Liu, D. Qin, P. Han, and C. Xu, "V2VSSC: A 3D semantic scene completion benchmark for perception with vehicle to vehicle communication," *arXiv preprint arXiv:2402.04671*, 2024.
- [65] R. Song, C. Liang, H. Cao, Z. Yan, W. Zimmer, M. Gross, A. Festag, and A. Knoll, "Collaborative semantic occupancy prediction with hybrid feature fusion in connected automated vehicles," in *CVPR*, 2024.
- [66] X. Wang, Z. Zhu, W. Xu, Y. Zhang, Y. Wei, X. Chi, Y. Ye, D. Du, J. Lu, and X. Wang, "OpenOccupancy: A large scale benchmark for surrounding semantic occupancy perception," in *ICCV*, 2023.
- [67] X. Tian, T. Jiang, L. Yun, Y. Wang, Y. Wang, and H. Zhao, "Occ3D: A large-scale 3D occupancy prediction benchmark for autonomous driving," in *NeurIPS*, 2023.
- [68] Y. Li, S. Li, X. Liu, M. Gong, K. Li, N. Chen, Z. Wang, Z. Li, T. Jiang, F. Yu, Y. Wang, H. Zhao, Z. Yu, and C. Feng, "SSCBench: A large-scale 3D semantic scene completion benchmark for autonomous driving," *arXiv preprint arXiv:2306.09001*, 2023.
- [69] A. Geiger, P. Lenz, and R. Urtasun, "Are we ready for autonomous driving? The KITTI vision benchmark suite," in *CVPR*, 2012.
- [70] H. Caesar, V. Bankiti, A. H. Lang, S. Vora, V. E. Liong, Q. Xu, A. Krishnan, Y. Pan, G. Baldan, and O. Beijbom, "nuScenes: A multimodal dataset for autonomous driving," in *CVPR*, 2020.
- [71] P. Sun, H. Kretzschmar, X. Dotiwalla, A. Chouard, V. Patnaik, P. Tsui, J. Guo, Y. Zhou, Y. Chai, B. Caine, V. Vasudevan, W. Han, J. Ngiam, H. Zhao, A. Timofeev, S. Ettinger, M. Krivokon, A. Gao, A. Joshi, Y. Zhang, J. Shlens, Z. Chen, and D. Anguelov, "Scalability in perception for autonomous driving: Waymo open dataset," in *CVPR*, 2020.
- [72] S. Wang, J. Zhu, and R. Zhang, "Meta-RangeSeg: LiDAR sequence semantic segmentation using multiple feature aggregation," *IEEE Robotics and Automation Letters*, 2022.
- [73] M. Aygun, A. Osep, M. Weber, M. Maximov, C. Stachniss, J. Behley, and L. Leal-Taixé, "4D panoptic LiDAR segmentation," in *CVPR*, 2021.
- [74] M. Najibi, J. Ji, Y. Zhou, C. R. Qi, X. Yan, S. Ettinger, and D. Anguelov, "Motion inspired unsupervised perception and prediction in autonomous driving," in *ECCV*, 2022.
- [75] J. Park, C. Xu, S. Yang, K. Keutzer, K. Kitani, M. Tomizuka, and W. Zhan, "Time will tell: New outlooks and a baseline for temporal multi-view 3D object detection," in *ICLR*, 2022.
- [76] Z. Pang, Z. Li, and N. Wang, "Model-free vehicle tracking and state estimation in point cloud sequences," in *IROS*, 2021.
- [77] Z. Xie, Z. Pang, and Y.-X. Wang, "MV-Map: Offboard HD map generation with multi-view consistency," in *ICCV*, 2023.
- [78] D. M. Hausman and J. Woodward, "Independence, invariance and the causal markov condition," *The British Journal for the Philosophy of Science*, 1999.
- [79] L. Yuan, Y. Chen, T. Wang, W. Yu, Y. Shi, Z. Jiang, F. E. Tay, J. Feng, and S. Yan, "Tokens-to-token ViT: Training vision transformers from scratch on ImageNet," in *ICCV*, 2021.
- [80] A. Dosovitskiy, L. Beyer, A. Kolesnikov, D. Weissenborn, X. Zhai, T. Unterthiner, M. Dehghani, M. Minderer, G. Heigold, S. Gelly, J. Uszkoreit, and N. Houlsby, "An image is worth 16x16 words: Transformers for image recognition at scale," in *ICLR*, 2021.
- [81] J. Yang, C. Li, P. Zhang, X. Dai, B. Xiao, L. Yuan, and J. Gao, "Focal attention for long-range interactions in vision transformers," in *NeurIPS*, 2021.
- [82] Y. Huang, W. Zheng, Y. Zhang, J. Zhou, and J. Lu, "Tri-perspective view for vision-based 3D semantic occupancy prediction," in *CVPR*, 2023.
- [83] X. Chen, K.-Y. Lin, C. Qian, G. Zeng, and H. Li, "3D sketch-aware semantic scene completion via semi-supervised structure prior," in *CVPR*, 2020.
- [84] J. Li, K. Han, P. Wang, Y. Liu, and X. Yuan, "Anisotropic convolutional networks for 3D semantic scene completion," in *CVPR*, 2020.
- [85] M. Berman, A. R. Triki, and M. B. Blaschko, "The lovász-softmax loss: A tractable surrogate for the optimization of the intersection-over-union measure in neural networks," in *CVPR*, 2018.
- [86] Y. Liao, J. Xie, and A. Geiger, "KITTI-360: A novel dataset and benchmarks for urban scene understanding in 2D and 3D," *IEEE Transactions on Pattern Analysis and Machine Intelligence*, 2023.
- [87] D. P. Kingma and J. Ba, "Adam: A method for stochastic optimization," in *ICLR*, 2015.
- [88] J. Zhang, H. Zhao, A. Yao, Y. Chen, L. Zhang, and H. Liao, "Efficient semantic scene completion network with spatial group convolution," in *ECCV*, 2018.